Journal of Colloid and Interface Science 629 (2023) 245–253

Contents lists available at ScienceDirect

Journal of Colloid and Interface Science

journal homepage: www.elsevier.com/locate/jcis

Creating lifting force in liquids via thermal gradients

Qingwen Dai [a,b,*], Jin Yan [a], Arman Sadeghi [c], Wei Huang [a], Xiaolei Wang [a], M.M. Khonsari [d,*]

[a] National Key Laboratory of Science and Technology on Helicopter Transmission, Nanjing University of Aeronautics and Astronautics, Nanjing 210016, China
[b] Institute for Nano- and Microfluidics, Technische Universität Darmstadt, Darmstadt 64287, Germany
[c] Department of Mechanical Engineering, University of Kurdistan, Sanandaj 66177-15175, Iran
[d] Department of Mechanical and Industrial Engineering, Louisiana State University, Baton Rouge, LA 70803, United States

GRAPHICAL ABSTRACT

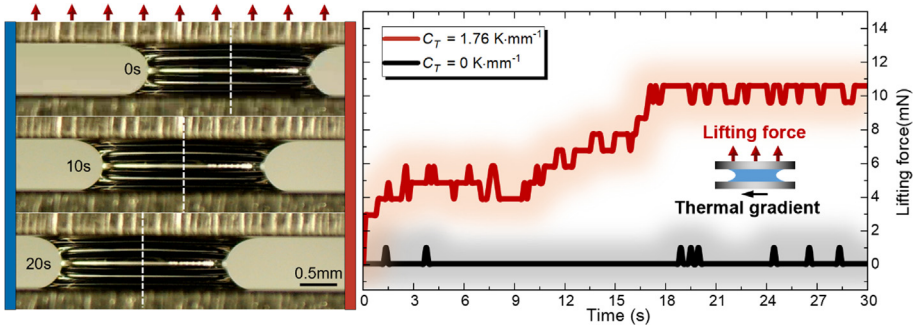

ARTICLE INFO

Article history:
Received 9 May 2022
Revised 31 August 2022
Accepted 1 September 2022
Available online 6 September 2022

Keywords:
Thermohydrodynamic effect
Liquid bridge
Thermocapillary flow
Couette flow
Lifting force

ABSTRACT

In this paper, we explore a concept and present the first experimental evidence to show that it is possible to form a stable liquid film and create lifting force at the interface via thermal gradient to minimize interfacial rubbing of surfaces and the associated wear. The approach is based on manipulating the flow behavior via thermocapillary, which describes how a liquid can be made to flow from warm to cold regions purely by inducing a thermal gradient. We show that liquid bridges between two parallel plates can be manipulated and stabilized under a combined effect of the thermocapillary flow and the Couette flow, which describes the motion of a viscous fluid between two parallel plates in a relative sliding motion. The equilibrium stage is confirmed under different experimental conditions of a thermal gradient, interfacial gap, liquid viscosity, and liquid bridge volume. A strategy is proposed to control liquid motion and create lifting force between two plates. A theoretical model is also presented to illustrate the principle of the equilibrium stage. Creating lifting forces at the interface offers a new thermohydrodynamic tool for manipulating liquids behavior. This approach has the potential for controlling liquid motion in mechanical components and nature.

1. Introduction

Nearly all transportation, power generation, manufacturing, and aerospace systems rely on complex arrays of mechanical assemblies with numerous moving parts and interacting surfaces that dissipate energy due to friction and wear. According to Luo et al. [1], the economic losses caused by these two factors account

* Corresponding author.
E-mail addresses: daiqingwen@nuaa.edu.cn (Q. Dai), knonsari@lsu.edu (M.M. Khonsari).

https://doi.org/10.1016/j.jcis.2022.09.002
0021-9797/

for approximately 2–7% of the gross domestic product (GDP) for modern countries every year, calling for improving the tribological performance of rubbing surfaces to combat the waste of energy [2,3].

Hydrostatic and hydrodynamic lubrication are two effective modes of lubrication, often used to separate the rubbing surfaces and reduce friction. The hydrodynamic model is more widely adopted since it does not require any auxiliary devices to maintain the liquid pressure. Nevertheless, for the hydrodynamic lubrication model to hold, three prerequisites must be satisfied: surfaces must be non-parallel, an adequate lubricant film must be available, and a relative motion between surfaces must exist [4,5]. Recent research shows that properly constructed microstructured patterns on surfaces can also generate hydrodynamic pressure between two parallel plates, thus extending the applicability of the hydrodynamic lubrication [6–10]. An intriguing question is whether it is possible to maintain effective lubrication and create a lifting force between two plates without altering the geometry of surfaces.

When a liquid is placed on a non-isothermal solid surface, an unbalanced surface tension force at the liquid–gas surface is created due to the temperature difference, promoting the liquid to flow from warm to cold regions, and this interfacial phenomenon is known as thermocapillary motion [11–23]. We propose that it is possible to create a lifting force by manipulating the thermocapillary effect. Furthermore, given that energy dissipates as heat [24], one can appropriately construct a thermal gradient to control the flow of liquid so that it can remain stationary at the desired location. In this paper, we explore this concept and present the first experimental evidence to show that it is possible to form a stable liquid film to minimize interfacial rubbing of surfaces and the associated wear. A theoretical model is also developed to gain insight and explore the mechanism of the equilibrium stage wherein thermal gradients can induce a lifting force between two parallel plates. Also highlighted are manipulating flows between plates in relative sliding motion with a wedged angle between them, offering potential application in various mechanical components and geological systems.

2. Materials and methods

2.1. Materials

Phenyl methyl siloxane (silicone oil) is widely used in engineering applications due to its excellent characteristic of thermal stability. Silicone oils with viscosities of 5, 20, 50, 100, and 1000 mPa·s were employed for testing; they were analytically pure and used as received (Aladdin, China). The solid plates were made of stainless steel 316 with dimensions of 90 × 14 × 1.5 mm (length × width × height) and average surface roughness of ~50 nm.

2.2. Methods

Fig. 1 shows the schematic of the designed experimental apparatus. Two stainless steel plates are arranged on a multidimensional mobile platform. It provides ~ 50 mm in length for fluid migration. The upper plate is held by a flexible fixture and a high accuracy force sensor (BMF-5, Dijia, China). They are mounted on rigid support equipped with an *x*-*z* mobile platform (XZM-40, Lianyi, China). The upper plate can slide in the *x*-direction, and the gap between the plates is adjustable. The force on the upper plate in the *z*-direction can be measured during the entire process. Two ends of the lower plate are fixed on heating and cooling elements embedded with two type-K thermocouples (accuracy of ± 1.5 K) to monitor the thermal gradient along the solid surface. The cooling element is stationary, and the heating one is fixed on a lifting platform. Thus, this apparatus enables one to efficiently perform experiments in parallel and wedged configurations.

Before experiments, all specimens were cleaned with ethanol, deionized water, and blow-dried with nitrogen. Next, after the desired thermal gradient is stabilized, silicone oil droplets are injected into the interface via a microsyringe within ~ 1 s, and the migration process from the side view is captured via a digital microscope (VHX-600, Keyence, Japan). Taking the central position of the liquid bridge as a reference, the migration distance and velocity are obtained. The inset in Fig. 1 shows a typical photograph of a liquid bridge that migrates from the hot to the cold side due to a thermal gradient. Via replacing the upper plate with a quartz glass, a bird's eye view of the migration process could be recorded, as shown in Fig. S1 and Movie S1. It is reasonable to regard the thermocapillary migration as a unidirectional motion, and its direction is defined as positive. The direction of the movement of the upper plate is defined as negative, since it can only move from the cold to the hot side. All experimental conditions are listed in Table 1.

3. Results and discussion

3.1. Thermocapillary and Couette flow between parallel plates

Fig. 2a shows the interfacial phenomena of a liquid bridge between the horizontal parallel plates subjected to a thermal gradient (C_T = 0.96 K·mm^{-1}), and the upper plate is stationary (the detailed process is shown in Movie S2). When the gap (h) between the plates is 0.8 mm, injecting a 10 μL silicone oil (η = 20 mPa·s) into the interface would form a liquid bridge there, and it migrates from the warm to the cold side. The migration distance linearly increases as time elapses, and the velocity increases rapidly within the initial 2 s and then stabilizes to 0.06 mm/s. When the gap (h) increases to 1.5 mm, a similar phenomenon is observed. However, the motion process is more intense than that of h = 0.8 mm, and the velocity stabilizes at 0.09 mm/s. This motion is known as thermocapillary flow, and the insets exhibit the dynamic process.

Fig. 2b shows an interfacial phenomenon of a liquid bridge between the horizontal parallel plates subjected to a sliding motion of the upper plate with no thermal gradient at the interface (Movie S3). Note that as the silicone oil is injected into the interface, it starts to move towards the negative direction induced by the motion of the upper plate, known as the Couette flow. Measurements show that after the initial 4 s, the velocity of the liquid bridge gradually increases to a constant value of −0.02 mm·s^{-1} with $U_{Upper\ plate}$ = -0.1 mm·s^{-1}, and to −0.07 mm·s^{-1} with $U_{Upper\ plate}$ = -0.2 mm·s^{-1}. Ignoring the initial several seconds, the velocities of the thermocapillary and the Couette flows are nearly constant. The details of the flow are presented in the insets.

Fig. 2c shows the behavior of the liquid bridge under combined Couette and thermocapillary flows (Movie S4). Keeping the upper plate stationary, a 10 μL liquid bridge migrates at the interface subjected to a thermal gradient. The initial velocity increases to 0.04 mm·s^{-1} within 6 s. As the upper plate starts to move in the negative direction ($U_{Upper\ plate}$ = -0.2 mm·s^{-1}), although the thermal gradient still exists, the velocity begins to gradually slow down until a critical point where the liquid bridge becomes stationary (8 ~ 10 s). Now, further increasing the $U_{Upper\ plate}$ to −0.3 mm·s^{-1} yields a reversed motion of the liquid bridge. The time-lapse photographs in Fig. 3c exhibit the dynamics of the flow between the plates: the liquid bridge moves in the positive direction initially and slows down gradually, and reversely moves at last.

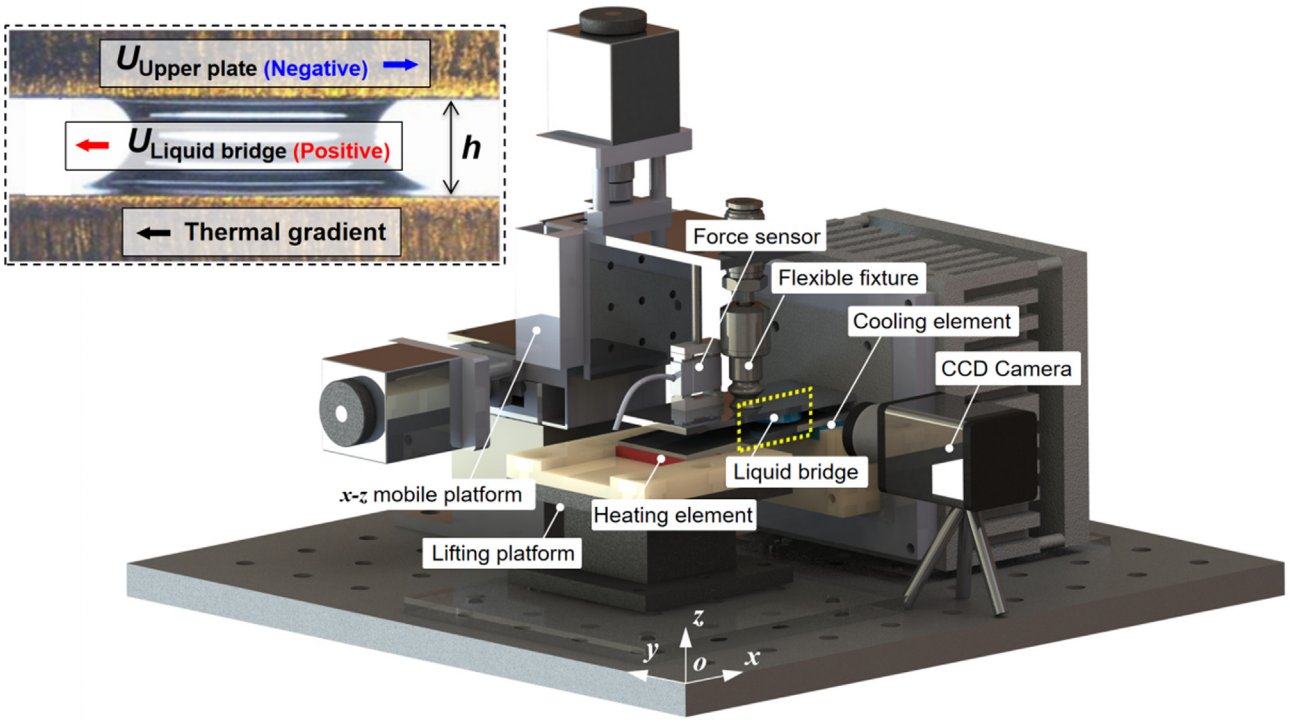

Fig. 1. Schematic of the apparatus and a photograph of a liquid bridge of silicone oil between two parallel plates.

Table 1
Experimental conditions.

Description	Symbol	Values
Thermal gradient	C_T	0 ~ 1.76 K·mm^{-1}
Gap between the plates	h	0.8, 1, 1.2, 1.5 mm
Volume of liquid bridge	V	10 μL
Dynamic viscosity of silicone oil	η	5, 10, 20, 50, 100, 1000 mPa·s
Surface tension of silicone oil	γ	20.6 ± 0.1 mN·m^{-1}
Density of silicone oil	ρ	949 ± 10 Kg·m^{-3}
Temperature derivative of surface tension	γ_T	0.00667 ± 0.005 mN·m^{-1}·K^{-1}
Wedge angle of the plates	β	0 ~ 1°
Velocity of the upper plate	$U_{Upper\ plate}$	0 ~ -0.5 mm·s^{-1}

3.2. Equilibrium between the thermocapillary and the Couette flows

The above results suggest that there exists a critical point where the thermocapillary flow and the Couette flow could offset each other. Additional experiments were carried out under different conditions to verify this point, and the results of which are shown in Fig. 3.

Fig. 3a shows the effect of viscosity on the interfacial flow. The upper part (positive y) represents the velocity of the liquid bridge and the lower part (negative y) displays the velocity of the upper plate. When C_T = 0.96 K·mm^{-1}, η = 20 mPa·s, h = 1.5 mm and $U_{Upper\ plate}$ = 0, the thermocapillary flow occurs ($U_{Liquid\ bridge}$ = 0.04 mm·s^{-1}). As the upper plate starts to move ($U_{Upper\ plate}$ = -0.2 mm·s^{-1} at 6 s), the velocity of the liquid bridge decreases. An equilibrium stage is reached between the thermocapillary flow and the Couette flow at 8 s, and the liquid bridge stops moving (green shaded region). Further increasing the $U_{Upper\ plate}$ to −0.3 mm·s^{-1} would yield a negative velocity of the liquid bridge. The thermocapillary flow recurs once the Couette flow disappears ($U_{Upper\ plate}$ = 0 after 16 s). A higher viscosity yields a weaker thermocapillary flow. For example, when η = 50 mPa·s, increasing the $U_{Upper\ plate}$ to −0.05 mm·s^{-1} (at 4 s) would gradually stop the motion of the liquid bridge (pink shaded region). There, the Couette flow overcomes the thermocapillary flow, resulting in a negative velocity of the liquid bridge.

Fig. 3b shows the effect of thermal gradient on the interfacial flow. When C_T = 0.96 K·mm^{-1}, the initial velocity of the liquid bridge is 0.04 mm·s^{-1}. As the $U_{Upper\ plate}$ is set to −0.2 mm·s^{-1} at 6 s, the liquid bridge slows down and stops (green shaded region). Further increasing the $U_{Upper\ plate}$ to −0.3 mm·s^{-1} yields a reverse motion of the liquid bridge. A higher thermal gradient promotes a faster motion. For example, when C_T = 1.36 K·mm^{-1}, a higher velocity of the upper plate is needed to impede the motion of the liquid bridge.

Fig. 3c shows the effect of the gap (h) between the plates on the interfacial flow. Note that a larger h contributes to a more intense thermocapillary flow. Correspondingly, a stronger Couette flow is needed to overcome it. Once the equilibrium stage between the thermocapillary flow and the Couette flow is reached, it can be maintained if all experimental conditions remain unchanged (green and pink shaded regions in Fig. 3c). If the velocity of the upper plate shifts to zero, the Couette flow disappears and the liquid bridge begins to migrate, as shown in Fig. 3c (red line after 18 s). A stable Couette flow can be formed if the velocity of the upper plate is maintained at a high value. See Fig. 3c (green line after 18 s).

3.3. Prediction of the equilibrium stage

The above experimental results reveal that there always exists a critical condition for a liquid bridge to become stationary and remain stable under the combined effects of the thermal gradient and the moving upper plate, i.e., there is an equilibrium stage between the thermocapillary flow and the Couette flow. In what follows, a theoretical model is developed to predict this equilibrium stage.

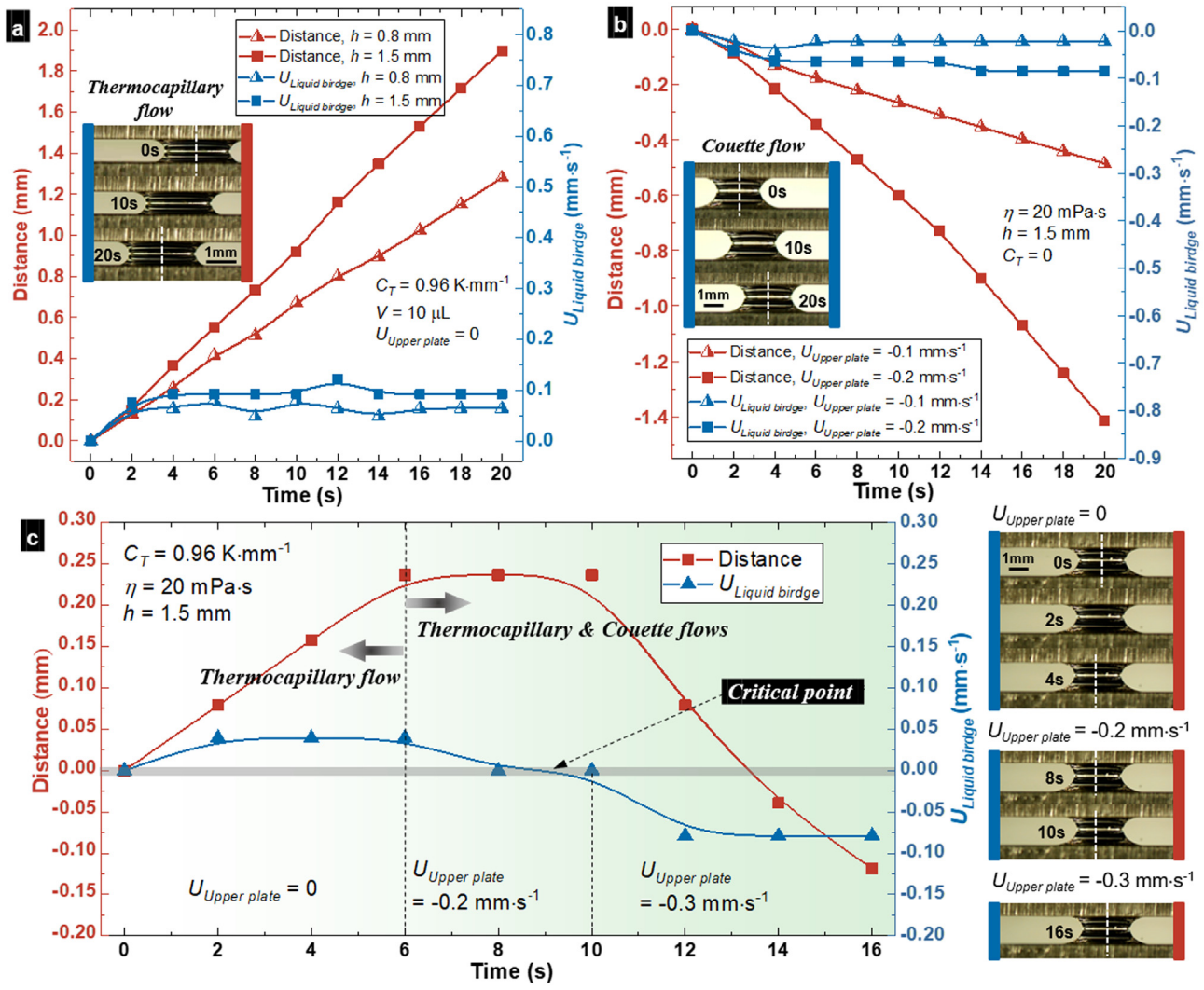

Fig. 2. Flow configurations of liquid bridges between the parallel plates: **(a)** motion induced by the thermocapillary effect, **(b)** motion induced by the moving upper plate, **(c)** motion induced by the combined action of the thermocapillary effect and the moving upper plate (C_T = 0.96 K·mm^{-1}, $U_{Upper\ plate}$ = 0 from 0 to 6 s, −0.2 mm·s^{-1} from 6 to 10 s, and −0.3 mm·s^{-1} from 10 to 16 s).

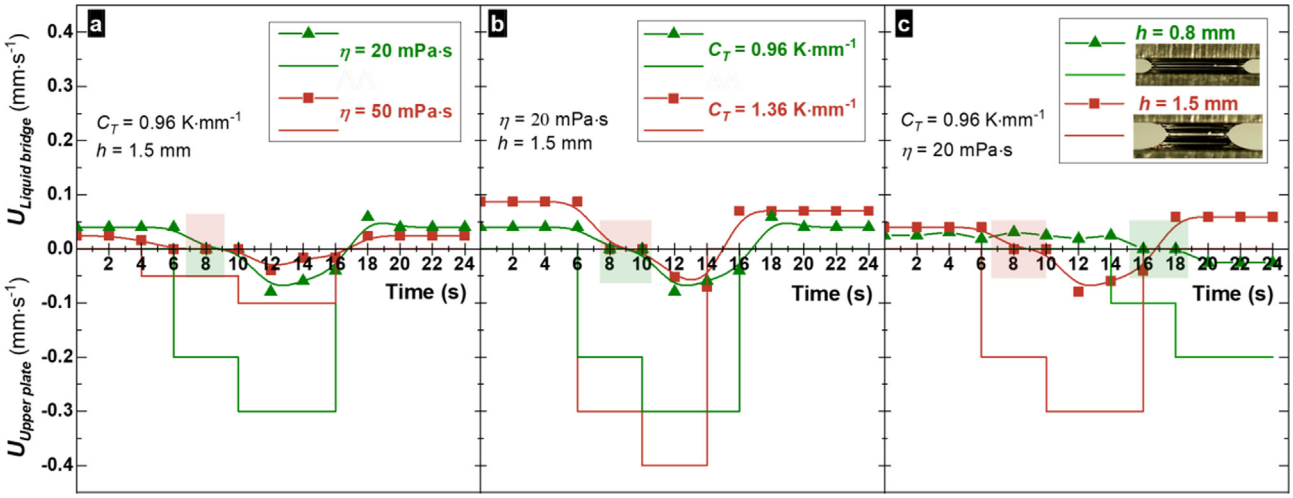

Fig. 3. The relationship between the thermocapillary flow and the Couette flow under different conditions: **(a)** viscosities (η) of 20 and 50 mPa·s, **(b)** thermal gradients (C_T) of 0.96 and 1.36 K·mm^{-1}, **(c)** gap sizes (h) of 0.8 and 1.5 mm.

For the investigated liquid bridges, the order of magnitudes of Reynolds number ($Re = \rho UL/\eta$) and Weber number ($We = \rho U^2 L/\gamma$) are $\sim 10^{-2}$ and $\sim 10^{-4}$, respectively (where ρ is the density, U is the velocity, L is the length of the footprint of the liquid bridge, and γ is the surface tension). These two dimensionless numbers are quite small, and it is reasonable to regard the motion of liquid bridges as a steady laminar flow. The mean order of magnitude of Capillary number ($Ca = \eta U/\gamma$) is $\sim 10^{-3}$, and the radius of the interface curvature of liquid bridges grows beyond the capillary length ($L_C = \sqrt{\gamma/\rho g}$, $\sim 10^{-3}$ m). Moreover, the mean order of magnitude of Bond number ($Bo = \rho g h^2/\gamma$, ~ 1) is also small. It is justified to assume that gravity has limited effect on the shape of the liquid bridge, that is, the menisci at the hot and cold sides are assumed to be circular arcs (Fig. 4). To check the validity of this assumption, the interface shape obtained from the side-view image with circular arcs was compared with the ideally symmetrical shape (see Fig. S2). Taking into account our requirements concerning the accuracy of the model, circular arcs represent the liquid surface with reasonable accuracy. Note that the duration of most migration experiments is less than 1 min. Evaporation loss test of silicone oil within 8 h was carried out and time-varying volume of liquid bridges within the experimental period was provided (as shown in Fig. S3). According to the results, it is reasonable to ignore the effect of evaporation.

Theoretical model. Fig. 4 shows the schematic of a liquid bridge between parallel plates. The cross-section through the center of the liquid bridge is chosen as a reference, the pressure drop P across the curved liquid–air interface can be described as follows.

$$P = \frac{\gamma}{R} = \frac{2\gamma \cdot \cos\theta}{h} \tag{1}$$

where γ is the surface tension of the liquid, h is the height of the liquid bridge, and θ is the contact angle.

The surface tension of a liquid decreases with increasing temperature and its variation can be approximated as.

$$\gamma = \gamma_0 + \gamma_T (T - T_0) \tag{2}$$

where γ_0 is the surface tension of the liquid at a reference temperature, T_0, and γ_T is the temperature derivative of the surface tension.

The thermal gradient is nearly constant on the solid surfaces, that is, $\frac{\partial T}{\partial x} = const = C_T$. The liquid surface is assumed to be in thermal equilibrium with the solid surfaces, and the initial movement when the liquid was first injected between the plates is ignored. The curved interface induced pressure difference ΔP between the cold and the hot side of a liquid bridge can be described as follows.

$$\Delta P = P_B - P_A = \frac{2(\gamma_B - \gamma_A)cos\theta}{h} = \frac{2C_T\gamma_T L cos\theta}{h} \tag{3}$$

Assuming that the end effects (close to the liquid surfaces), and the velocity components in the y and z directions are negligible, the momentum equation reduces to:

$$\frac{\partial^2 u}{\partial z^2} = \frac{1}{\eta}\frac{\partial P}{\partial x} = \frac{1}{\eta}\frac{\Delta P}{L} \tag{4}$$

where u is the velocity component in the x-direction, and η is the dynamic viscosity.

Assuming no-slip boundary condition at the two surfaces, we have:

$$\begin{cases} u = 0, z = 0 \\ u = U_{\text{Upper plate}}, z = h \end{cases} \tag{5}$$

Integrating Eq. (4) and applying the boundary conditions given in Eq. (5), we arrive at the velocity field of the liquid bridge. The result is:

$$u(z) = \frac{1}{2\eta}\frac{\Delta P}{L}(z^2 - zh) + \frac{U_{\text{Upper plate}}}{h}z \tag{6}$$

Substituting for ΔP in Eq. (6) form Eq. (3), the average velocity of the liquid bridge can be obtained as follows.

$$U_{\text{Liquid bridge}} = \frac{1}{h}\int_0^h u(z)dz = \frac{1}{2}U_{\text{Upper plate}} + \frac{C_T\gamma_T h cos\theta}{6\eta} \tag{7}$$

Substituting$U_{\text{Liquid bridge}}$ = 0, we arrive at the critical condition when the equilibrium stage is reached. The result is:

$$U_{\text{Upper plate}} = -\frac{C_T\gamma_T h cos\theta}{3\eta} \tag{8}$$

With the above formula, one could easily predict the critical velocity of the upper plate. Viewing from the hydrodynamics, the Marangoni effect is a flow of a liquid due to the gradient in the surface tension of the liquid, and the Marangoni number ($Ma = T_\Delta \gamma_T h/\eta\kappa$) is usually used to determine its stability (where T_Δ is the temperature difference,$T_\Delta = C_T L$, and κ is the thermal diffusivity of silicone oil, $\sim$0.0826 mm^2·s^{-1}). Hereby, the dimensionless number (Ma) is adopted to evaluate the Marangoni and Couette flows, that is:

$$U_{\text{Upper plate}} = -\frac{\kappa \cos\theta}{3L} \cdot Ma \tag{9}$$

This equation presents a general relationship between the Marangoni and Couette flows, of which the footprint (L) is in positive correlation with the volume of the liquid bridge (V). Referring to

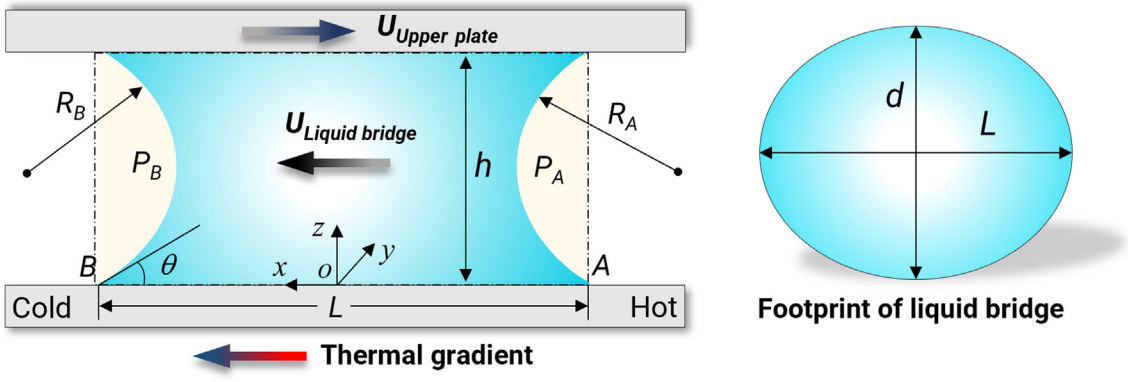

Fig. 4. Schematic of a liquid bridge between parallel plates and its footprint.

Fig. S1, it is believed that the footprint on the upper and lower plates is ellipse, and the aspect ratio can be directly calculated from these images. Thus, we have [25]:

$$\frac{x^2}{\left(\frac{L}{2}\right)^2}+\frac{y^2}{\left(\frac{L}{2\delta}\right)^2}=1 \tag{10}$$

$$\delta=\frac{L}{d}\approx 1+0.069Bo \tag{11}$$

where δ is the ratio of semi-minor axis length. Generally, the volume of the liquid bridge equals to the volume of the elliptic cylinder (dash line shown in Fig. 4) minus the volume of two hemispheroids (yellow zones shown in Fig. 4), thus:

$$V=\frac{1}{4}\pi Ldh-\frac{1}{6}\pi h^3=\frac{\pi L^2 h}{4(1+0.069Bo)}-\frac{1}{6}\pi h^3 \tag{12}$$

Then, the footprint (L) can be obtained as a function of volume (V):

$$L=\sqrt{\frac{4\left(V+\frac{1}{6}\pi h^3\right)(1+0.069B_o)}{\pi h}} \tag{13}$$

Verification. In what follows, a comprehensive comparison between the theoretical the experimental critical velocities of the upper plate ($U_{\text{Upper plate}}$) under different conditions is presented. Eq. (8) can be used to predict the critical velocity of the upper plate when the thermocapillary flow equilibrates to the Couette flow.

Fig. 5a shows both the theoretical and experimental results for the critical velocity of the upper plate ($U_{\text{Upper plate}}$) plotted as a function of viscosity. Note that the critical $U_{\text{Upper plate}}$ decreases rapidly with increasing viscosity since a higher viscosity yields a more significant viscous resistance. Fig. 5b shows the critical $U_{\text{Upper plate}}$ plotted as a function of the thermal gradient. Generally, a larger thermal gradient yields a more substantial thermal flow; thus, a higher velocity of the upper plate is needed to stop the motion of the liquid bridge. Fig. 5c shows the effect of the gap size (h) on the critical velocity. For a liquid bridge with a constant volume, the length of the footprint (L) is inversely proportional to h, a smaller L results in a faster migration velocity. As a result, a higher $U_{\text{Upper plate}}$ is needed to reach the equilibrium stage. Moreover, according to Eq. (9), the theoretical critical velocity of the upper plate ($U_{\text{Upper plate}}$) was plotted as a function of the Marangoni number (Ma) alongside the experimental data. As shown in Fig. 5d, the absolute value of the $U_{\text{Upper plate}}$ increases with increasing Ma, and experimental data under different conditions fit the numerical results well. Overall, the migration velocity trends reach unanimity, and the agreement further establishes the validity of the theoretical model.

Although slight differences exist between the theoretical and the experimental data at some points, most of the theoretical predictions agree with the experimental data both in trend and magnitude. Therefore, the validity of the derived theoretical expression of the velocity of the upper plate, given by Eq. (8) is confirmed.

3.4. Lifting force at the interface between parallel and wedged surfaces

One of the most important purposes of maintaining liquids between solid surfaces is to enhance the tribological performance. Having demonstrated that we can manipulate liquid bridges at the interfaces via balancing the interfacial thermal flow and the Couette flow, we now proceed to investigate the thermal flow related

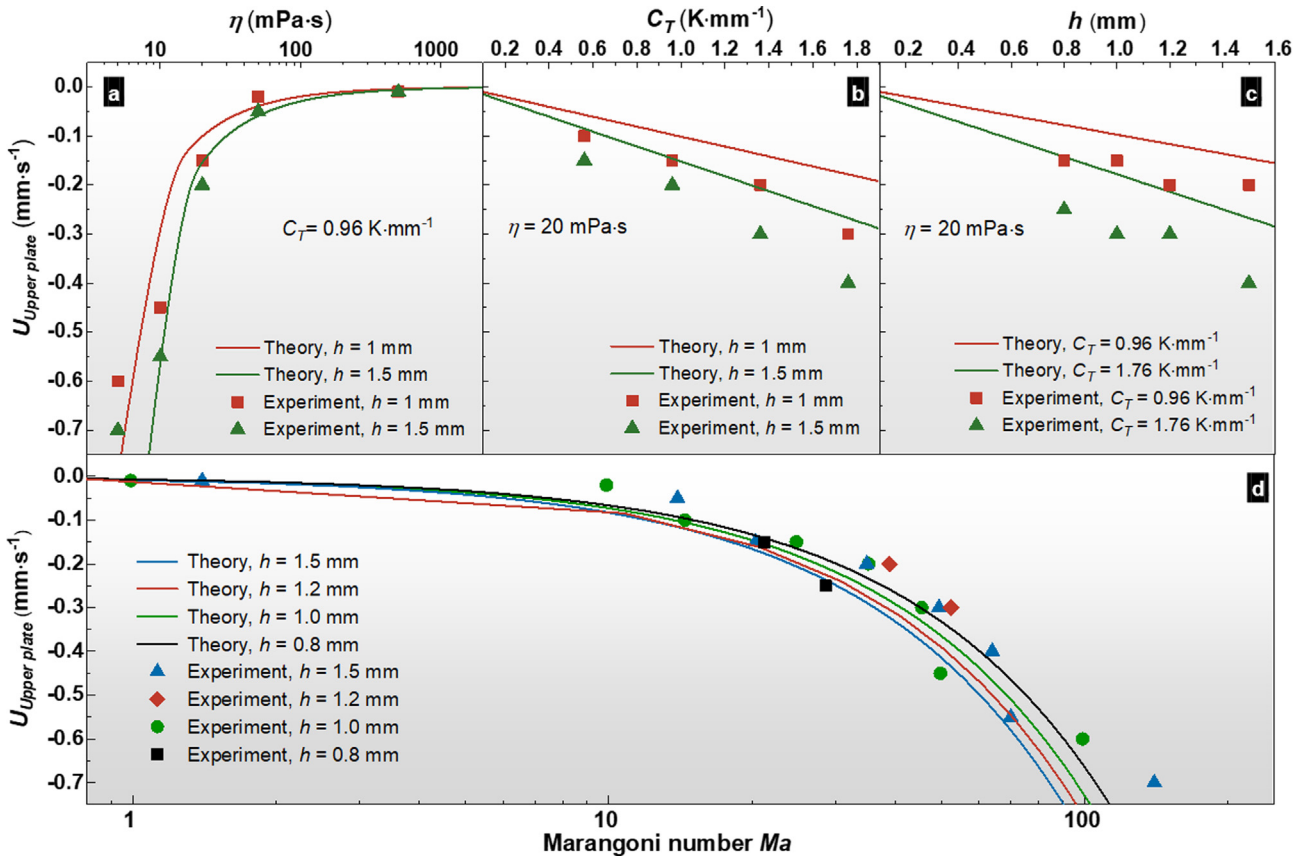

Fig. 5. Comparison between the theoretical predictions of the equilibrium stage between the thermocapillary flow and the Couette flow and the experimental results under different conditions: $U_{\text{Upper plate}}$ plotted as a function of **(a)** viscosity, **(b)** thermal gradient, **(c)** gap size, and **(d)** Marangoni number.

to the forces at the interfaces, of which the lifting and pulling forces denote the upward and downward driving force on the upper plate, respectively.

Fig. 6a shows the liquid bridges (η = 20 mPa·s, C_T = 0, $U_{\text{Upper plate}}$ = 0) generated negative force between two wedged and stationary plates, and a typical result is provided in Movie S5. The gap (h = 0.8 mm) is defined as the initial distance between the two plates at the wedged side. The liquid bridge does not move and no force is generated between the parallel plates. When β = 0.6°, the liquid bridge spontaneously moves towards the convergent wedge direction and generates a force of −5 mN, and this force increases to −12 mN as β increases to 1°. Referring to the inset in Fig. 6a, when the two plates are wedged, the radius of curvature of the meniscus on the left side (R_1) is smaller than that on the right side (R_2). Thus, Laplace pressure drop (ΔP_{La}) exists at the interface, which can be approximated as $\Delta P_{\text{La}} = \gamma_1/R_1 - \gamma_2/R_2$. Since the liquid–air interface bends toward the interior of the liquid, the Laplace pressure points to the air. This pressure drop (ΔP_{La}) actuates the local motion and generates a liquid bridge force to adhere the two plates. Consequently, a pulling force is formed. The ΔP_{La} increases with increasing wedge angle (β), and the pulling force increases correspondingly.

A similar situation is observed when the upper plate begins to slide, as shown in Fig. 6b. A liquid bridge (C_T = 0, β = 0°, h = 0.8 mm, η = 20 mPa·s) at the interface can generate a pulling force of −3 mN when$U_{\text{Upper plate}}$ = -0.1 mm·s^{-1}, and this force increases with increasing $U_{\text{Upper plate}}$ (-14 mN at a speed of −0.3 mm·s^{-1}). Referring to Fig. 6f, once the upper plate moves, Couette flow occurs, and the liquid bridge starts to move so that the upper part of the liquid bridge drags the lower part to move together. Thus, the flow can be regarded as a viscous force-induced laminar flow, and the wetting and de-wetting process just exists at the interface between the liquid bridge and the lower plate. The interfacial tensions are constant ($\gamma_1 = \gamma_2 = \gamma_3$), and the liquid bridge force at the interface acts as the pulling force on the two plates.

It is interesting to observe in Fig. 6c that when applying a thermal gradient, liquid bridges (η = 20 mPa·s, h = 0.8 mm) can create a significant lifting force even if the two plates are parallel and stationary. This force increases with increasing the thermal gradient, which is approximately 11 mN when C_T = 1.76 K·mm^{-1}. These data reveal that thermocapillary migration can generate a lifting force at the interface. This is manifested as a thermohydrodynamic effect. Referring to Fig. 6g, when a thermal gradient is applied to the interface, thermocapillary flow occurs, the wetting and de-wetting processes exist at both the upper and the lower three-phase interfaces. This is different from the Couette flow shown in Fig. 6f. As the migration progresses, the front edge of the liquid bridge needs to overcome the pinning effect. Thus, the liquid tends to gather at the front edge of the liquid bridge (from 1 to 3 in Fig. 6f), yielding a deformation of the meniscus. Moreover, since the surface tension increases with decreasing temperature, the relationship of $\gamma_1 < \gamma_2 < \gamma_3$ holds. As a result, an inner pressure is generated, providing a supporting force. Note that the all experiments were carried out on smooth surfaces. Nevertheless, it is believed that the contact angle hysteresis effect will influence the lifting force [26,27], which could further contribute to the pinning effect, enhancing the lifting force.

This thermohydrodynamic effect was further confirmed by examining the flow between two wedged plates. As shown in

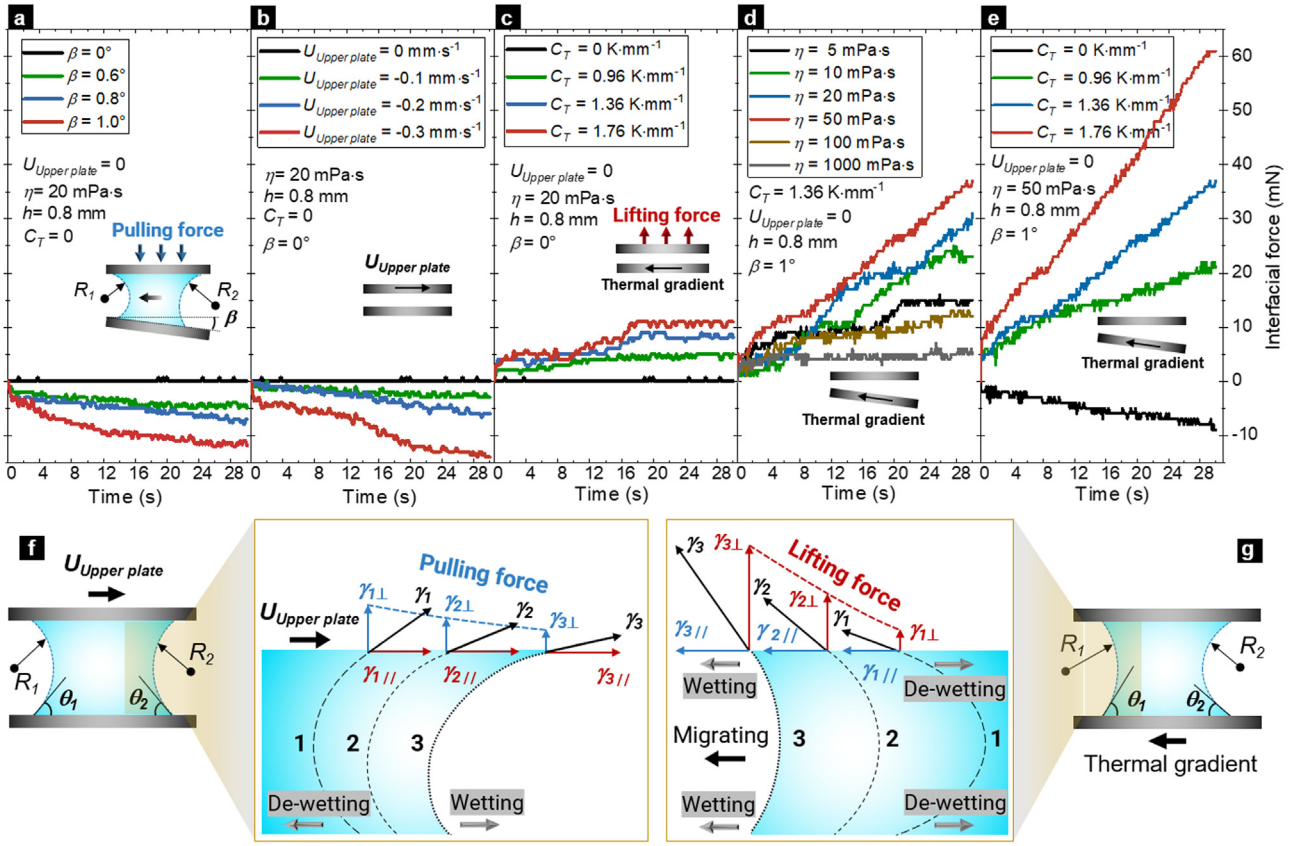

Fig. 6. Lifting force at the interface under conditions of: (a) varying wedge angle (β), C_T = 0, and $U_{\text{Upper plate}}$ = 0; (b) varying velocity of the upper plate ($U_{\text{Upper plate}}$), C_T = 0, and $\beta = 0^{\circ}$; (c) varying thermal gradient (C_T), $\beta = 0^{\circ}$, and $U_{\text{Upper plate}}$ = 0; (d) varying thermal gradient (C_T), $\beta = 1^{\circ}$, and $U_{\text{Upper plate}}$ = 0; (e) varying viscosity (η), C_T = 0.96 K·mm^{-1}, $\beta = 1^{\circ}$, and $U_{\text{Upper plate}}$ = 0.

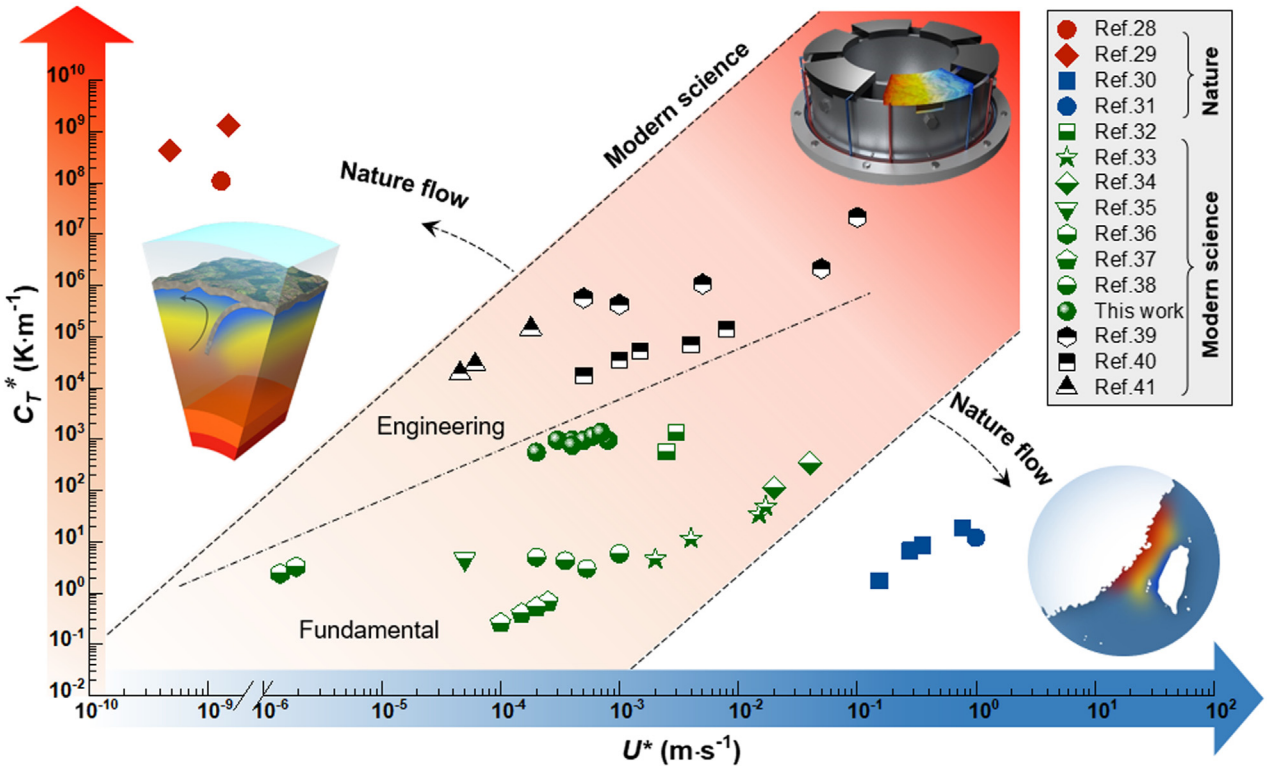

Fig. 7. A blueprint of using a thermal gradient (C_T^*) to manipulate different types of liquid motions (U^*) from modern science to nature.

Fig. 6d and 6e (Movie S6), the magnitude of the generated force is much higher than that between two parallel plates. Fig. 6d shows the effect of viscosity on the thermohydrodynamic effect, silicone oils with different viscosities of 5, 10, 20, 50, 100 and 1000 mPa·s are compared. Under experimental conditions of C_T = 0.96 K·mm^{-1}, h = 0.8 mm, and β = 1°, silicone oil with a viscosity (η) of 5 mPa·s yields a lifting force of 15 mN, and this force increases to as high as 38 mN when η = 50 mPa·s. When further increasing the viscosity to 1000 mPa·s, the liquid bridge does not move between the interface, resulting in a negligible lifting force. This is because the internal frictional resistance of liquids is proportional to the viscosity, and a thermal gradient of 1.36 K·mm^{-1} cannot actuate the thermocapillary migration of the liquid bridge (η = 1000 mPa·s). Fig. 6e shows the effect of thermal gradient on the thermohydrodynamic effect, when the two plates are initialized with a wedge angle (β) of 1°, a liquid bridge (η = 50 mPa·s, h = 0.8 mm) subjected to a thermal gradient of 1.76 K·mm^{-1} (red line in Fig. 6e) yields a lifting force of 62 mN, which is 6 times higher than the absolute value of that for C_T = 0° (black line in Fig. 6e). Generally, the thermohydrodynamic effect is enhanced at the wedged interface.

4. Applications and outlook

The data suggest that by using an external thermal gradient, one could generate a considerable lifting force between two parallel or wedged surfaces. This fundamental principle opens a new window for future research for controlling the motion of liquids in internal flows, which has extensive application prospects in modern machinery. For example, in lightly-loaded fluid-film bearings, introducing this thermohydrodynamic effect could enhance the hydrodynamic lubrication by generating a lifting force that could decrease the shaft vibrations and friction coefficient. In a mechanical seal, one may use this principle to enhance sealing performance and prevent the leakage of hazardous liquid into the environment. Besides, the general principle will likely inspire complementary theoretical and experimental studies on the topic of rheology.

It is also worthwhile to note that if the velocity of a liquid at the surface or interface is already known, one could apply a thermal gradient (C_T^*) at the surface or interface to stabilize the motion and reach an equilibrium position. Referring to Eq. (8), the expected thermal gradient (C_T^*) can be approximated as:

$$C_T^* = \frac{3\eta U^*}{\gamma_T h^* \cos\theta} \tag{14}$$

where U^* is the relative velocity of the liquid, h^* is the characteristic dimension of the liquid.

Manipulation of liquid motion has wide applications in various fields. In nature, super spatial scale liquid flows widely exist, where the fluid migration in the mantle wedge influences the mineral grain size and mantle compaction [28], or even induces the plate movement [29]. Thermocapillary flows can be adapted to control the ocean currents [30,31] to change the earth's climate. In general, the ability to control the motion of a liquid is of fundamental importance in research laboratories [32–38] and engineering applications of mechanical components that must operate safely in extreme conditions [39–41]. According to Eq. (14), we envision a blueprint of using temperature differences to manipulate different types of flows that can benefit from manipulating flows. As shown in Fig. 7, it can be referred from this figure that adopting an appropriate thermal gradient (C_T^*) would be a feasible technique to manipulate liquid motions both in nature and in modern science.

5. Conclusions

This study proposed a manipulation strategy of adopting thermal gradients to control liquid motions and create lifting forces

between two plates. The thermocapillary motion describes a flow of a viscous liquid from warm to cold regions on a non-isothermal solid surface [11–23]. Couette flow is a flow of a viscous fluid at the interface of two solid surfaces, one of which is moving tangentially relative to the other [4,5]. Our experimental investigations revealed that liquid bridges can be manipulated and stabilized between two parallel plates under the thermocapillary and Couette flow combined. The effects of a thermal gradient, interfacial gap, liquid viscosity, and volume of liquid bridges on the equilibrium state were discussed. A theoretical model was established to predict the equilibrium stage between the thermocapillary and the Couette flows. The present model agreed well with the experiment in predicting the critical velocity of the upper plate to maintain the liquid bridges at the interface under different conditions. The capability to manipulate liquids and create lifting forces at the interface is manifested as a thermohydrodynamic effect, which is vital for controlling liquid flow in both natural and engineered systems.

Declaration of Competing Interest

The authors declare that they have no known competing financial interests or personal relationships that could have appeared to influence the work reported in this paper.

Acknowledgments

The authors (Q.D., J. Y., W.H., and X.W.) are grateful for the support provided by the National Natural Science Foundation of China (No. 51805252); Q.D. and A.S. acknowledge the support from the Alexander von Humboldt Foundation.

Appendix A. Supplementary data

Supplementary data to this article can be found online at https://doi.org/10.1016/j.jcis.2022.09.002.

References

[1] J.B. Luo, M. Liu, Origin of friction and the new frictionless technology—superlubricity: Advancements and future outlook, Nano Energy 86 (2021) 106092.
[2] P.G. Grützmacher, A. Rosenkranz, A. Szurdak, F. König, G. Jacobs, G. Hirt, F. Mücklich, From lab to application - improved frictional performance of journal bearings induced by single- and multi-scale surface patterns, Tribol. Int. 127 (2018) 500–508.
[3] F. Zhou, Y. Wu, A novel insight into lubrication, Tribology 36 (2016) 132–136.
[4] J. Frêne, D. Nicolas, B. Degueurce, D. Berthe, M. Godet, Hydrodynamic lubrication: Bearings and thrust bearings, Elsevier, 1997.
[5] M.M. Khonsari, E.R. Booser, in: Applied tribology: Bearing design and lubrication, John Wiley & Sons, 2017.
[6] A. Kovalchenko, O. Ajayi, A. Erdemir, G. Fenske, I. Etsion, The effect of laser surface texturing on transitions in lubrication regimes during unidirectional sliding contact, Tribol. Int. 38 (3) (2005) 219–225.
[7] C. Shen, M.M. Khonsari, Tribological and sealing performance of laser pocketed piston rings in a diesel engine, Tribol. Lett. 64 (2016) 26.
[8] D. Gropper, L. Wang, T.J. Harvey, Hydrodynamic lubrication of textured surfaces: A review of modeling techniques and key findings, Tribol. Int. 94 (2016) 509–529.
[9] P.G. Grützmacher, A. Rosenkranz, S. Rammacher, C. Gachot, F. Mücklich, The influence of centrifugal forces on friction and wear in rotational sliding, Tribol. Int. 116 (2017) 256–263.
[10] X.L. Wang, K. Adachi, K. Otsuka, K. Kato, Optimization of the surface texture for silicon carbide sliding in water, Appl. Surf. Sci. 253 (3) (2006) 1282–1286.
[11] L.E. Scriven, C.V. Sternling, The marangoni effects, Nature 187 (4733) (1960) 186–188.
[12] K.D. Barton, R. Shankar Subramanian, The migration of liquid drops in a vertical temperature gradient, J. Colloid Interf. Sci. 133 (1) (1989) 211–222.
[13] S. Daniel, M.K. Chaudhury, J.C. Chen, Fast drop movements resulting from the phase change on a gradient surface, Science 291 (5504) (2001) 633–636.
[14] Q.W. Dai, M.M. Khonsari, C. Shen, W. Huang, X.L. Wang, Thermocapillary migration of liquid droplets induced by a unidirectional thermal gradient, Langmuir 32 (30) (2016) 7485–7492.
[15] R. Tadmor, Marangoni flow revisited, J. Colloid Interf. Sci. 332 (2) (2009) 451–454.
[16] S. Kumar, Liquid transfer in printing processes: Liquid bridges with moving contact lines, Annu. Rev. Fluid Mech. 47 (1) (2015) 67–94.
[17] J.B. Bostwick, P.H. Steen, Stability of constrained capillary surfaces, Annu. Rev. Fluid Mech. 47 (1) (2015) 539–568.
[18] E. Bormashenko, Physics of wetting : Phenomena and applications of fluids on surfaces, De Gruyter, 2017.
[19] P.G. Grützmacher, A. Rosenkranz, A. Szurdak, C. Gachot, G. Hirt, F. Mücklich, Lubricant migration on stainless steel induced by bio-inspired multi-scale surface patterns, Mater. Design 150 (2018) 55–63.
[20] Q.W. Dai, W. Huang, X.L. Wang, M.M. Khonsari, Directional interfacial motion of liquids: Fundamentals, evaluations, and manipulation strategies, Tribol. Int. 154 (2021) 106749.
[21] J.M. Montanero, A. Ponce-Torres, Review on the dynamics of isothermal liquid bridges, Appl Mech Rev 72 (2020) 010803.
[22] X.L. Yang, K. Zhuang, Y. Lu, X.L. Wang, Creation of topological ultraslippery surfaces for droplet motion control, ACS Nano 15 (2) (2021) 2589–2599.
[23] K. Zhuang, X.L. Yang, W. Huang, Q.W. Dai, X.L. Wang, Efficient bubble transport on bioinspired topological ultraslippery surfaces, ACS Appl. Mater. Inter. 13 (51) (2021) 61780–61788.
[24] M. Amiri, M.M. Khonsari, On the thermodynamics of friction and wear-a review, Entropy 12 (2010) 1021–1049.
[25] J.W. Harris, H. Stocker, Handbook of mathematics and computational science, Springer New York, USA, 1998.
[26] Q.W. Dai, W. Huang, X.L. Wang, Contact angle hysteresis effect on the thermocapillary migration of liquid droplets, J. Colloid Interf. Sci. 515 (2018) 32–38.
[27] E. Bormashenko, Progress in understanding wetting transitions on rough surfaces, Adv. Colloid Interface Sci. 222 (2015) 92–103.
[28] N.G. Cerpa, I. Wada, C.R. Wilson, Fluid migration in the mantle wedge: Influence of mineral grain size and mantle compaction, Journal of Geophysical Research: Solid Earth 122 (8) (2017) 6247–6268.
[29] M.I. Billen, M. Gurnis, A low viscosity wedge in subduction zones, Earth. Planet. Sc. Lett 193 (1-2) (2001) 227–236.
[30] A. Constantin, Frictional effects in wind-driven ocean currents, Geophysical & Astrophysical Fluid Dynamics 115 (1) (2021) 1–14.
[31] N.H. Kumagai, J. García Molinos, H. Yamano, S. Takao, M. Fujii, Y. Yamanaka, Ocean currents and herbivory drive macroalgae-to-coral community shift under climate warming, Proc. Natl. Acad. Sci. 115 (36) (2018) 8990–8995.
[32] Q.W. Dai, Y.J. Ji, Z.J. Chong, W. Huang, X.L. Wang, Manipulating thermocapillary migration via superoleophobic surfaces with wedge shaped superoleophilic grooves, J. Colloid Interf. Sci. 557 (2019) 837–844.
[33] J. Hartmann, M.T. Schür, S. Hardt, Manipulation and control of droplets on surfaces in a homogeneous electric field, Nat. Commun. 13 (2022) 289.
[34] Y. Sumino, N. Magome, T. Hamada, K. Yoshikawa, Self-running droplet: Emergence of regular motion from nonequilibrium noise, Phys. Rev. Lett. 94 (2005) 068301–68311.
[35] K. Ichimura, S.-K. Oh, M. Nakagawa, Light-driven motion of liquids on a photoresponsive surface, Science 288 (5471) (2000) 1624–1626.
[36] L. Hauer, W.S.Y. Wong, V. Donadei, K.I. Hegner, L. Kondic, D. Vollmer, How frost forms and grows on lubricated micro- and nanostructured surfaces, ACS Nano 15 (3) (2021) 4658–4668.
[37] P. Lazar, H. Riegler, Reversible self-propelled droplet movement: A new driving mechanism, Phys. Rev. Lett. 95 (2005) 4.
[38] Q.W. Dai, S.Q. Chen, W.Huang, X.L. Wang, S. Hardt, On the thermocapillary migration between parallel plates. *Int. J. Heat Mass Tran.* **2022**, 182: 121962.
[39] X.M. Li, F. Guo, P.L. Wong, Y. Zhao, Regulation of lubricant supply by wettability gradient in rolling ehl contacts, Tribol. Int. 120 (2018) 565–574.
[40] P.G. Grützmacher, A. Rosenkranz, E. Atalay, A. Szurdak, C. Gachot, G. Hirt, F. Mücklich, Guiding lubricant on stainless steel surfaces by channel-like structures fabricated by roller- and micro-coining, Physica A 505 (2018) 482–489.
[41] Ling, Y., Fullana, J.-M., Popinet, S., Josserand, C. Droplet migration in a hele–shaw cell: Effect of the lubrication film on the droplet dynamics. *Phys. Fluids* **2016**, 28: 062001.